Structural Insights into the Conformational Variability of FtsZ

María A. Oliva, Daniel Trambaiolo and Jan Löwe*.

MRC Laboratory of Molecular Biology
Hills Road, Cambridge
CB2 2QH, UK

*corresponding author
Jan Löwe
MRC Laboratory of Molecular Biology
Hills Road, Cambridge
CB2 2QH, UK
phone: +44 1223 252969
fax: +44 1223 213556
jyl@mrc-lmb.cam.ac.uk

ABSTRACT

FtsZ is a prokaryotic homologue of the eukaryotic cytoskeletal protein tubulin and plays a central role in prokaryotic cell division. Both FtsZ and tubulin are known to pass through cycles of polymerization and depolymerization, but the structural mechanisms underlying this cycle remain to be explored. Comparison of tubulin structures obtained in different states has led to a model in which the tubulin monomer undergoes a conformational switch between a "straight" form found in the walls of microtubules and a "curved" form associated with depolymerization, and it was recently proposed that this model may also apply to FtsZ. In this paper we present new structures of FtsZ from *Aquifex aeolicus*, *Bacillus subtilis, Methanococcus jannaschii* and *Pseudomonas aeruginosa* that provide strong constraints on any proposed role for a conformational switch in the FtsZ monomer. By comparing the full range of FtsZ structures determined in different crystal forms and nucleotide states and in the presence or absence of regulatory proteins, we find no evidence of a conformational change involving domain movement. Our new structural data make it clear that the previously proposed "straight" and "curved" conformations of FtsZ were related to inter-species differences in domain orientation rather than two interconvertible conformations. We propose a new model in which lateral interactions help determine the curvature of protofilaments.

INTRODUCTION

FtsZ is a highly conserved cytoskeletal protein involved in bacterial cell division. FtsZ is the first protein known to localize to the division site, where it polymerizes to form a dynamic ring structure known as the Z ring [1; 2]. The polymerization dynamics of FtsZ depend on its properties as a GTPase: nucleotide binding promotes longitudinal association of monomers into protofilaments, while hydrolysis leads to protofilament disassembly [3; 4; 5]. Despite extensive investigations into FtsZ behaviour both *in vivo* and *in vitro*, its precise role and mechanism in cell division remain unclear [6; 7; 8; 9]. Recent evidence suggests that in addition to its role in septum formation, FtsZ may also play a role in cell wall elongation [10; 11; 12].

The monomer and protofilament structures of FtsZ are similar to those of its eukaryotic homologue tubulin [13; 14; 15], and improved understanding of the mechanisms of each of these proteins may yield insights that are relevant to the other. Tubulin αβ-heterodimers assemble into microtubules, which are long hollow cylinders composed of laterally associated straight protofilaments. The GTPase activity of β-tubulin is activated in the polymer, and the dynamic instability of microtubules arises from the fact that the thermodynamically unstable GDP-bound protofilaments are held in a metastable polymerized state by lateral interactions and the presence of a GTP-bound cap. Loss of the GTP cap leads to rapid depolymerization of the microtubule. Dynamic instability requires that GDP in the polymer cannot exchange with GTP. The mechanics of depolymerization are thought to play a role in generating the force for sister chromatid separation during mitosis [16; 17; 18].

FtsZ monomers form protofilaments that are similar to those of tubulin; although lateral association of FtsZ protofilaments has been observed *in vitro*, the molecular details and physiological relevance of this bundling are unclear [19; 20]. FtsZ protofilaments can be straight or curved, and other morphologies including sheets, tubes, minirings and helices have also been observed *in vitro* depending on the experimental conditions used [21; 22]. In contrast to tubulin, FtsZ filaments are thought not to display dynamic instability, and biochemical experiments suggest that FtsZ polymers undergo rapid exchange of either nucleotide or monomers, either of which would be incompatible with dynamic instability [23; 24]. It is not currently known

whether the Z ring plays a direct mechanical role in cell division or merely serves as a scaffold for the recruitment of other cell division proteins.

FtsZ and tubulin share a distinctive fold with a two-domain architecture: an N-terminal nucleotide-binding domain is connected via a central helix (H7) to a C-terminal domain that is involved in forming the protofilament [13; 14]. The GTPase active site is formed at the interface between monomers by insertion of acidic residues from the C-terminal domain's T7 (synergy) loop into the nucleotide-binding pocket of the preceding monomer in the protofilament. In the case of FtsZ, the unit of polymerization is the monomer, while in the case of tubulin it is the αβ-tubulin heterodimer. Both α- and β-tubulin each bind one nucleotide molecule. α-tubulin remains GTP-bound and stably associated with β-tubulin because the T7 loop of β-tubulin lacks the acidic residue that would be needed to complete α-tubulin's active site [14].

Structures of tubulin in different states reveal the existence of distinct conformations of the tubulin monomer: a "straight" conformation found in the straight protofilaments of microtubules and flat Zn-induced sheets [14; 25], and a "curved" conformation seen in co-crystals of αβ-tubulin with colchicine and the RB3 stathmin-like domain [26] and in helical ribbons [27]. A similar conformation has been observed in the γ-tubulin [28] and the bacterial tubulin homologues BtubA/B [29]. The conformational switch involves a change in the packing angle between tubulin's N-terminal and C-terminal domains (8º in α-tubulin and 11º in β-tubulin) coupled with a shift in the position of the central helix H7 (1.5 Å in α-tubulin and 2.5 Å in β-tubulin). Somewhat surprisingly, both the α and β-tubulin subunits of the tubulin heterodimer seem to undergo this switch in concerted fashion, despite the fact that only β-tubulin alters its nucleotide state. This observation seems to suggest that the tubulin conformational switch, unlike the classical conformational switches seen in small GTPases [30; 31; 32; 33], is dependent on the longitudinal and lateral interactions between monomers rather than on nucleotide content alone. It has been proposed that the conformational switch plays a role in force generation by depolymerizing microtubules, perhaps acting as a power stroke as the protofilament curls outwards from the microtubule wall [34; 35].

Does FtsZ undergo a conformational switch similar to that proposed for tubulin? We previously determined structures of *Methanococcus jannaschii* FtsZ (MjFtsZ) in different nucleotide states and found no evidence of significant

conformational changes, despite the fact that the crystal packing in one crystal form creates interfaces between monomers similar to those found in the protofilament [36]. However, a recent comprehensive analysis of all available FtsZ structures found that the conformation of *Pseudomonas aeruginosa* FtsZ (PaFtsZ) bound to the inhibitory protein SulA differed from the conformations of free FtsZ protein from other species in a manner that resembled the tubulin straight-curved conformational switch [37]. The authors of this study proposed that SulA binding might switch the conformation of FtsZ from a "curved" to a "straight" state by mimicking the protofilament contacts, although the functional relevance of this was unclear.

Here, we present the structures of FtsZ from two new organisms, *Bacillus subtilis* (BsFtsZ) and *Aquifex aeolicus* (AaFtsZ), as well as the structure of free FtsZ from *P. aeruginosa* and a new high-resolution structure of free *Methanococcus jannaschii* FtsZ (MjFtsZ), and analyse the implications of these new structures for our understanding of FtsZ conformational mechanics. The structure of *B. subtilis* FtsZ shows no unusual features, but we find that crystals of *A. aeolicus* FtsZ contain an alternative mode of packing at the protofilament interface, suggesting the degree of flexibility that this interface might be able to accommodate. Comparison of the structures of SulA-bound and free *P. aeruginosa* FtsZ reveals no significant conformational changes, and we conclude that the differences between *P. aeruginosa* and *M. jannaschii* FtsZ are due simply to their different primary sequences rather than the presence of a conformational switch that depends on the nucleotide state of the monomeric protein. A comprehensive structural analysis of all available structures reveals the intrinsic variability of the relative positioning of between N-terminal and C-terminal domains in FtsZ from different species. Finally, we present a model for the FtsZ polymerization cycle, taking into account the lack of a nucleotide-dependent conformational change in the monomer.

RESULTS AND DISCUSION

Structure of FtsZ from *B. subtilis*

We have solved the structure of untagged, full-length *B. subtilis* FtsZ at a resolution of 2.2 Å (Figure 1A). Although the crystals only grew in the presence of the inhibitor dichamanetin [38], we were unable to locate the inhibitor in the final electron density maps. The overall structure of BsFtsZ is similar to previously solved FtsZ structures. No electron density was visible for the N-terminal residues 1 to 12 or the C-terminal residues 316 to 382. The structure shows BsFtsZ in its empty form: nucleotide content analysis of the protein used for crystallization yielded a GXP:FtsZ ratio of 0.07, and the crystallographic electron density maps show that the nucleotide-binding pocket is empty apart from a bound sulfate ion. It is worth highlighting that the nucleotide-binding pocket is blocked by helix H2 and T3 loop of the next molecule in the crystal lattice, which make impossible dichamanetin or nucleotide soaking experiments.

High-resolution structure of FtsZ from *M. jannaschii*

We have solved MjFtsZ in a new crystal form that yielded diffraction data to 1.7 Å resolution. The electron density maps revealed the presence of GDP in the nucleotide-binding pocket, without magnesium ion. Helix H0 is in a different position when compared with PDB ID 1FSZ. After aligning the N-terminal domains, the key residues in the C-terminal domains (Table 2) show an rmsd of 1.2 Å. This difference between two structures in the same nucleotide state but in different crystal contexts gives an indication of the inherent flexibility of the FtsZ monomer.

Structure of FtsZ from *A. aeolicus*

FtsZ from *Aquifex aeolicus* was crystallized as a C-terminally truncated construct lacking residues 331-367, since full-length protein produced only poor quality crystals and primary sequence analysis suggested that these residues were likely to be unstructured. The AaFtsZ crystals diffracted to a resolution of 1.7 Å (Figure 1A). The crystals contain one molecule of AaFtsZ per asymmetric unit, and electron density is clearly defined for residues 5 to 331 and bound GDP.

The packing of the AaFtsZ molecules in the crystal is somewhat similar to the arrangement thought to occur in the protofilament (Figure 1B). We have suggested previously that the best high-resolution model for the FtsZ protofilament is found in

crystals of the GTP/Mg^{2+} soaked form of MjFtsZ (PDB ID 1W5A): one dimer seen in these crystals is closely similar to the αβ-tubulin dimer, and the two aspartic acid residues in the T7 loop, which are known to form part of the protofilament's active site, are positioned to activate a water molecule for nucleophilic attack on the γ-phosphate [36]. The new AaFtsZ crystals contain an interface between the monomers that is similar to the interface seen in the MjFtsZ dimer, although the contact area is less extensive. The repeat distance between AaFtsZ monomers is 44 Å, slightly longer than the 43 Å spacing seen in the crystallographic dimer of MjFtsZ and the 42-43 Å distance measured by electron microscopy of EcFtsZ and MjFtsZ sheets [20; 39]. The adjacent monomers are positioned such that the two residues Asp206 and Asp209 of the synergy loop involved in catalysis are shifted away from the active site. Asp206 forms a salt bridge with Lys139, whose positive charge is widely conserved in FtsZ from different species.

The differences between the pseudo-protofilament interfaces in MjFtsZ and AaFtsZ crystals may be partly related to nucleotide state. It is possible to soak GTP into the MjFtsZ crystals and the structure that results appears to be poised in preparation for catalysis: the crystal packing was thus interpreted as representing the GTP-bound form of the protofilament. The AaFtsZ crystals were grown in the presence of GDP and contain GDP in the active site, and it was not possible to obtain a GTP-bound form by soaking. However, we have recently managed to obtain co-crystals of AaFtsZ with the inhibitor 8-morpholino-GTP, again at very high resolution (1.4 Å, in collaboration with Tanneke den Blaauwen, Amsterdam, manuscript in preparation). Despite the additional presence of the nucleotide γ-phosphate and a bound magnesium ion, these crystals are essentially identical to the GDP-bound crystals that we describe here. The lack of a conformational change in AaFtsZ induced by the presence of the γ-phosphate reinforces the previously reported observation that monomeric FtsZ shows no structural changes between its empty, GDP-bound and GTP-bound forms [36].

The observation of an unsually long repeat distance is reminiscent of the extension of the repeat distance in tubulin following hydrolysis of GTP to GDP [40], and the movement of the catalytic aspartic acid residues away from the active site is not entirely surprising if the crystal packing mimics the post-hydrolysis state of the protofilament. The docking interface between adjacent monomers in true

protofilaments may permit greater flexibility than is commonly assumed. Similar flexibility in the protofilament interface can be seen by comparing the different αβ-tubulin structures determined by electron crystallography of Zn-induced sheets [14; 35], electron microscopic reconstruction of helical tubes formed in the presence of GDP or GMPPCP [41] and X-ray crystallography of αβ-tubulin in complex with the RB3 stahmin-like domain and colchicine [26]. These changes in docking between tubulin monomers contribute substantially to the curvature of tubulin protofilaments in their curved state, in addition to some flexibility within the subunits, and it is likely that the same is true of FtsZ.

Structure of SulA-free FtsZ from *Pseudomonas aeruginosa*

PaFtsZ was crystallized in the absence of SulA using the previously described C-terminally truncated construct lacking 76 residues [42]. Crystals containing a single molecule per asymmetric unit diffracted to a resolution of 2.9 Å, and the structure was solved by molecular replacement (Figure 1A). Nucleotide content of the purified protein showed a GXP/FtsZ ratio of 0.35 after gel filtration, and electron density maps indicated the presence of GDP in the nucleotide-binding pocket. Magnesium was not present in the crystallization conditions, and no magnesium ion was visible in the electron density maps.

Superposition of FtsZ structures and determination of domain angles

We aligned all previously available and new FtsZ structures (Table 1) using 56 residues from the core secondary structural elements of the highly conserved N-terminal domain (Table 2). The domain-swapped dimer of *Thermotoga maritima* FtsZ (TmFtsZ) and one chain of *Mycobacterium tuberculosis* FtsZ (MtFtsZ) were excluded from the analysis since these structures contain distortions due to the changes in loop T7 (TmFtsZ) or crystal contacts (MtFtsZ) that are unlikely to be physiologically relevant. When performing pairwise alignments of structures it is possible to introduce bias towards the reference structure. Therefore, we first carried out the alignment using PaFtsZ as a reference and then generated averaged Cα positions of the 56 key residues from all the aligned structures (Figure 2, table 2). Finally, the averaged Cα positions were used as the reference for alignment of all structures. Having aligned the FtsZ structures in this way, it is possible to detect subtle shifts in

the relative positions of the N-terminal and C-terminal domains that would not be evident if the structures were aligned over the entire molecule.

Lack of conformational change between free and SulA-bound *P. aeruginosa* FtsZ

The previously determined structure of PaFtsZ in complex with SulA shows a SulA dimer bound to two FtsZ molecules [42]. SulA binds to and occludes the T7 loop surface of the FtsZ monomer, blocking the protofilament interface and preventing polymerization [43]. However, a recent analysis by Buey et al. (2006) found that superposition of MjFtsZ and PaFtsZ structures reveals a displacement of the H7 helix coupled with a movement of the C-terminal domain. Since this difference was reminiscent of the conformational changes thought to occur in the curved-to-straight conformational switch of tubulin, the authors concluded that MjFtsZ crystals show the monomer in its 'curved' state while the PaFtsZ-SulA complex shows the monomer its a 'straight' state. They further proposed that SulA binding, in addition to blocking the protofilament interface, might induce a conformational change that mimics the conformation of FtsZ in straight protofilaments. However, these conclusions remained tentative in the absence of structural data on SulA-free PaFtsZ.

A comparison of our new structure of SulA-free PaFtsZ with the previously published PaFtsZ-SulA complex shows no significant difference between the two (Figure 3), despite the different crystal contexts. Any changes seen between the two structures are much smaller than the ones seen between FtsZ structures from different organisms (see below, figure 4 and tables 3, 4). Comparison of the structure of SulA-free PaFtsZ with the two PaFtsZ molecules in the asymmetric unit of the SulA-bound crystals shows that the differences between the SulA-free and SulA-bound structures are not greater than the differences between the two SulA-bound structures. The superposition of SulA-free FtsZ with SulA-bound molecule A shows that differences with chain A only involve small displacements of S2, loop T3, loop T7 (in N-terminus domain) and S9, S10 and loops in protein surface (in C-terminus domain) with an rmsd of 0.5 Å. Within molecule B, shifts localize in H1, H2, H2-S3 loop, H5, H6, H7 top, T7 loop (N-terminus domain) and S9, S10 and loops on the protein surface (in C-terminal domain) with a slightly bigger rmsd of 0.9 Å. The domain rotations of the C-terminal domain after alignment of the N-terminal domains of the free and SulA-bound structures are 2.59º (with chain A) and 2.09º (with chain B). Comparing the two molecules from the SulA-bound crystals, the largest changes

involve H6, the top of H7 (N-terminal domain) and H9, H10, H9-S8 loop, S9-H10 loop (C-terminal domain) with an rmsd of 0.8 Å.

It therefore appears that SulA inhibits FtsZ polymerisation simply by blocking the protofilament interface and preventing longitudinal association, rather than by inducing any substantial conformational change.

Absence of a nucleotide-dependent conformational change

It has been proposed that tubulin undergoes a nucleotide-dependent conformational change and that this causes changes in the resulting polymer structures [34]. For FtsZ, we have previously favoured a model that does not invoke such changes because no significant differences were observed between the crystal structures of MjFtsZ in the GDP and GTP states (PDB ID 1FSZ and 1W5E), [36]. Analogous findings were reported in the case of γ-tubulin [28].

Here we use the improved structural alignment of all available structures of MjFtsZ in different nucleotide states (Table 3). GDP-bound (PDB ID 1FSZ) and GTP-bound mutant MjFtsZ (W319Y, PDB ID 1W5E) show an rmsd between their C-terminal domains of 1.0 Å and we consider this difference insignificant, taking the resolutions of the structures into account. Similarily, our new pair of AaFtsZ:GDP and AaFtsZ:8-morpholino-GTP show even smaller differences (rmsd 0.2 Å). We therefore conclude that there are no changes of the inter-domain angle in the monomer caused by changes in nucleotide state.

A slightly larger difference is seen between the GDP-bound state of the monomer of MjFtsZ (PDB ID 1FSZ) and the nucleotide-free form in the pseudo-protofilaments (PDB ID 1W59) involving an rmsd of 1.45 Å (Figure 4A). The differences between these two structures could be due either to the nucleotide content or to the protofilament-like crystal packing, or both. Since the two different crystal forms of MjFtsZ-GDP have an rmsd for the C-terminal domain of 1.2 Å, we would consider that the differences shown in Figure 4A represent only the inherent flexibility of the FtsZ monomer rather than a nucleotide-dependent change.

Soaking experiments with different nucleotides also revealed no conformational change on FtsZ, as is expected since the crystal lattice imposes strong constraints. For example, a GMPCPP soak of previously GDP-containing MjFtsZ crystals shows an rmsd of only 0.4 Å (PDB IDs 1W58, 1FSZ).

Domain arrangements in other FtsZs

A comprehensive analysis of the superposed structures of FtsZ from different organisms and in different states reveals that the most striking pairwise differences are seen in the comparisons between PaFtsZ and MjFtsZ, with a Cα rmsd of 2.67 Å calculated over the C-terminal domain (larger than the 1.84 Å rmsd reported in the previous analysis [37], as these used a slightly different set of residues to align the N-terminal domain), PaFtsZ and BsFtsZ with a Cα rmsd of 2.39 Å and AaFtsZ and BsFtsZ with an rmsd of 2.17 Å (Table 3 and figure 4B). These deviations are induced by a general downward movement of PaFtsZ C-terminal domain followed by a sideways displacement of the top of H7 helix (Figure 4A). The rotation angle of the C-terminal domain shows the same trend as the Cα rmsd measurements (Table 4): the biggest difference in angle is observed between PaFtsZ and MjFtsZ (8.02º); the rotation angles of the PaFtsZ C-terminal domain relative to BsFtsZ, AaFtsZ and MtFtsZ are 7.6º, 7.4º and 5.8º respectively. The differences in the position of helix H7 relative to the N-terminal domain can be seen clearly by examining the position of the nucleotide in the different structures (figure 4C) where the guanosine forms a hydrogen bond with a conserved Asp residue in helix H7, and differences in the position of this helix relative to the N-terminal domain lead to slightly different orientations of the nucleotide.

PaFtsZ and MjFtsZ show the biggest differences in C-terminal domain position, while BsFtsZ, MtFtsZ and AaFtsZ display an intermediate position between the two extremes. BsFtsZ is closer to MjFtsZ with an rmsd of 1.63 Å, while AaFtsZ is closer to PaFtsZ with an rmsd of 1.52 Å. MtFtsZ has a C-terminal domain position roughly intermediate between PaFtsZ and MjFtsZ, with rmsd values of 1.7 Å and 1.63 Å respectively. These rmsd values are an average of all those from FtsZ structures of a single organism when it is applicable (Table 3). This comparison shows clear evidence of structural differences among FtsZ homologues from different organisms. These differences do not appear to correlate with phylogenetic groupings, crystallisation conditions or truncations of the construct used for crystallization, and probably represent no more than the natural differences between structures that would be expected on the basis of their different primary sequences. Sequence alignments of

these FtsZ homologues shows an identity of 33% to 54%, of which most similarity is located in the N-terminal domain.

'Lattice vs Strain' model

The structural data and analysis presented here suggest a revised model of the straight-to-curved transition in the protofilament (Figure 5). Although it is possible that future structural data on FtsZ may reveal a nucleotide-induced conformational change in the monomer, we consider this highly unlikely given the fact that we have analysed a large number of structures from several different species, in different nucleotide states (GTP, GDP and empty) and in the presence and absence of bound inhibitory proteins, and found no evidence of such a conformational change. In the tubulin field, this relates to similar data obtained with γ-tubulin [28].

Central to our proposal is the observation that FtsZ monomers (and probably tubulin as well) and the protofilament interfaces contain flexibility that allows the molecules to balance different sources and sinks of energy in the system. Starting with the GDP form of the monomer, the immediate effect of GDP to GTP exchange is to promote longitudinal association of monomers into protofilaments; no conformational change in the monomer takes place at this stage. Once formed, the protofilaments will have some flexibility and can adopt different curvatures by bending at the interfaces between subunits and perhaps within the subunits themselves [26; 44]. In higher-order structures formed by lateral association of single protofilaments, the strain of curvature can be offset by the energy of the lateral interactions. The currently accepted view of protofilament structure is that the GDP-bound form of the protofilament is intrinsically curved while the GTP-bound form is straight. However, the majority of experimental data on filaments of both FtsZ and tubulin have been obtained in the presence of interactions that may alter the filament curvature: crystal packing, bundling of filaments or adsorption onto EM grids. We believe that current proposals for the structure of the single protofilament remain speculative.

High-resolution structural information is missing for two crucial states of our model. For FtsZ, there is currently no structural model of the protofilament in a state that has appropriate lateral interactions. An experimentally determined structure of FtsZ in laterally associated filaments could reveal details of changes at the protofilament interface and perhaps also within the monomer. These changes might

include a shift in the angle between the N-terminal and C-terminal domains similar to that observed for tubulin.

Similarly, we expect that a high-resolution structure of αβ-tubulin in the absence of lateral interactions would reveal the free conformation of the tubulin dimer. This would allow us to decide whether the tubulin dimer is intrinsically curved in the absence of additional sources of energy (stathmin binding or lateral interactions) and whether this conformation indeed involves changes in the angle between the N-terminal and C-terminal domain. Unfortunately, both structures, FtsZ in straight protofilaments and free tubulin are currently not available.

METHODS

Protein Expression and Purification

FtsZ from *M. jannaschii* was expressed and purified as described earlier [36].

FtsZ from *P. aeruginosa* (1-318) was cloned as described [42]. The protein was purified as described [45] (method 1, ammonium sulfate precipitation) with minor modifications. After 30% amonium sulfate precipitation and anion exchange chromatography, the protein was dialyzed against 50 mM Tris-HCl, pH 8.0, 200 mM KCl, 1 mM EDTA, 10 % glycerol and gel filtrated in the same buffer using a Sephacryl S200 26/60 column (Amersham). The purest fractions were concentrated to 10 g/L and directly used for crystallization. The nucleotide content was measured as described [20].

Untagged, full length *ftsZ* from *B. subtilis* (ATCC 23857D) was cloned into *NdeI* and *BamHI* of pHis17. Sequencing of multiple independent clones revealed three modifications relative to the published database sequence: *cgc* to *cgt* (a silent mutation in the codon for R332), *gac* to *gag* (D350E) and *gca* to *cca* (A351P). These changes were assumed to be due to strain differences or errors in the database sequence. The protein was purified by 30% ammonium sulfate precipitation in 50 mM Tris-HCl, pH 8.0, 50 mM KCl, 1 mM EDTA, 10 mM $MgCl_2$, followed by anion exchange chromatography with a 5 mL HiTrap Q HP column (Amersham) in 50 mM MES-KOH, pH 6.5, 5 mM $MgCl_2$ where FtsZ was eluted with 300 mM KCl. Finally the protein was gel filtrated (Sephacryl S300 26/60 column, Amersham) in 50 mM Tris-HCl, pH 7.5, 1 mM EDTA, 1 mM NaN_3, concentrated to 15 g/L and stored at –80 °C.

C-terminally truncated *A. aeolicus* FtsZ (residues 1-330) was cloned into *NdeI* and *BamHI* of pHis17, yielding a C-terminally His_6-tagged fusion protein. The protein was expressed in *E. coli* BL21-AI cells (Invitrogen). Exponential phase cells (OD_{600}= 0.7) were induced for 4 hours by the addition of 0.3 % arabinose. The protein was purified by HisTrap nickel affinity chromatography followed by gel filtration on a Sephacryl S200 column in 20 mM Tris-HCl pH 7.5, 1 mM EDTA and 1 mM NaN_3. Fractions containing highly pure FtsZ were concentrated to 15 g/L and stored at –80°C.

Crystallization and structure determination

All crystals were grown at 19°C using the sitting drop vapour diffusion technique and initial hits were found using our in-house nanolitre crystallization facility [46]. Diffraction data was collected at the ESRF (Grenoble, France). Data was integrated and reduced using MOSFLM and SCALA [47]. Structure solution and refeniment were performed using CNS [48] or REFMAC [49].

MjFtsZ (MJZ crystal form) crystals were grown over a reserboir solutio ncontaining 0.1 M Bis-Tris propane, pH 7.0 and 4.0 M ammonium acetate. Drops were composed of 100 nl of protein at 10.0 g/L (with 8 mM $MgCl_2$, 8 mM NaF, 200 µM $AlCl_3$, 1 mM GDP) and 100 nl of reservoir solution (AlF_3 was not visible in the electron density). Crystals were cryo protected with 25 % glycerol. The structure was solved by molecular replacement with 1FSZ as model.

PaFtsZ crystals were grown over a reservoir solution containing 0.1 M BisTris, pH 5.8, 26 % PEG2000MME. Drops were composed of 200 nl of protein (10.0 g/L) and 200 nl of reservoir solution. Cryobuffer was 15% PEG200. Molecular replacement was carried out using the PaFtsZ monomer from PDB ID 1OFU as a search model.

BsFtsZ crystals were grown over a reservoir solution containing 0.1 M MES-NaOH pH 6.0, 0.24 M $(NH_4)_2SO_4$, 11% PEG8000 and drops were composed of 500 nL of protein plus 500 nL of reservoir. Before flash cooling, the crystals were placed in mother liquor plus 15 % glycerol. Molecular replacement was carried out using the PaFtsZ monomer as a search model (PDB ID 1OFU).

AaFtsZ crystals were grown by adding 2 mM $MgCl_2$ and 1 mM GDP to the protein sample (15 g/L) and crystallizing over a reservoir solution containing 0.1 M MOPS-NaOH pH 6.5, 0.2 M NaCl, 28% PEG400. Drops were composed of 500 nL protein solution plus 500 nL reservoir. No additional cryoprotectant was added to the crystals prior to flash freezing. Diffraction data were collected to 1.7 Å on a Rigaku RU-300 rotating anode. Molecular replacement was performed with MjFtsZ (PDB ID 1FSZ) as search model.

Alignment of FtsZ structures.

To select the core secondary structure residues of the N-terminal domain, we performed an initial multiple structural alignment of FtsZ homologues from *P. aeruginosa*, *A. aeolicus*, *B. subtilis*, *M. tuberculosis*, *M. jannaschii* and *T. maritima* FtsZ using the MSDFold web server [50]. We selected 56 core residues that are located within secondary structure elements of the N-terminal domain of FtsZ, choosing those residues that were less than 2 Å apart in the alignment and were located in the interior of the protein, thus excluding regions of the structure that might be distorted by crystal contacts (see figure 2, grey arrows). All structures were aligned based on these core residues against PaFtsZ (PDB ID 1OFU) and superimposed. We then calculated the average Cα coordinates for the 56 residues of the N-terminal domain core and used these as a new reference pdb file for all structures, including PaFtsZ in a second round of alignment.

Rmsd values of the C-terminal domains after aligning the N-terminal domains were calculated using 11 carefully selected residues located on core secondary structural elements of that domain (see figure 2, black arrows). Rotation angles were calculated using the same residues.

FIGURES

Figure 1

(A) Ribbon representation of FtsZ structures from *M. jannaschii*, *P. aeruginosa* (residues 2-316), *A. aeolicus* (residues 4-326) and *B. subtilis* (residues 12-315). The nucleotide-binding domain is coloured dark/light blue, the core helix H7 yellow, and the C-terminal domain red/orange. (B) Protofilament-like structures in crystals of GDP-bound *A. aeolicus* FtsZ (PDB ID XXXX) and empty *M. jannaschii* FtsZ (PDB ID 1W59). The protofilament interface is altered by a sliding movement of the top subunit with respect to the lower subunit in the *Aquifex* structure (left) and is distorted by a rotation of about 10° in the *Methanococcus* structure (right).

Figure 2

M. jannaschii FtsZ amino acid sequence and secondary structure. Secondary structure elements in the N-terminal domain are coloured dark/light blue, the central helix H7 is yellow and secondary structure elements in the C-terminal domain are in red/orange. Grey arrows in the nucleotide-binding domain indicate the core residues of the N-terminal domain chosen for structural alignments. Black arrows in the C-terminal domain indicate residues selected for calculating relative rmsd and rotation angles between the C-terminal domains.

Figure 3

Ribbon representation of *P. aeruginosa* structure superposition in side (A) and top view (B). FtsZ in complex with the cell division inhibitor SulA is in dark-red (PDB ID 1OFU) and FtsZ without SulA (PDB ID XXXX) is in blue. Both molecules have GDP in the nucleotide-binding pocket, shown in space-filling representation. FtsZ without SulA shows a 2.59° downward movement of the C-terminal domain. The lack of significant changes when comparing the free and SulA-bound form of FtsZ excludes a conformational change as proposed [37].

Figure 4

FtsZ structural superpositions. (A) Pairwise superposition of GDP-MjFtsZ (PDB ID 1FSZ) in dark green and empty MjFtsZ (PDB ID 1W59 chain A) in red showing the biggest structural differences when comparing two FtsZ structures from the same

organism (rmsd 1.45 Å, 4.72° rotation). (B) Pairwise comparison of GDP-PaFtsZ without SulA (PDB ID XXXX) in dark blue with GDP-MjFtsZ (PDB entry 1FSZ) in dark green (left), empty BsFtsZ (PDB ID XXXX) in light blue (second from left), GDP-AaFtsZ (PDB ID XXXX) in orange (third from left) and GDP-MtFtsZ (PDB ID 1RQ7 chain A) in brown (right). After aligning the nucleotide-binding domains, the C-terminal domains show upward movements from 1.46 Å to 2.39 Å. The same trend is reflected when calculating single rotation angles that vary between 5.88° to 8.02° between different FtsZ molecules. (C) GDP-bound PaFtsZ, MjFtsZ, AaFtsZ and MtFtsZ superposition showing the nucleotide-binding pocket. The guanine base of GDP points at a conserved Asp residue in helix H7 (Asp187, Asp212, Asp179 and Asp184 respectively). No large changes can be seen, but the position of the base moves slightly due to the different position of H7 and the aspartic acid residues.

Figure 5

Schematic drawing of the 'Lattice vs Strain' model. The central idea is that lateral interactions can stabilise a strained conformation of the protofilament. The monomer shows no change in conformation related to the nucleotide state. Single protofilaments may prefer to adopt straight or curved conformations depending on the nucleotide state. Increasing or decreasing the curvature introduces some degree of strain, which may result in distortion of the protofilament interface or the monomer conformation. In higher-order structures formed by lateral association of single protofilaments, the strain of curvature can be offset by the energy of the lateral interactions.

ACKNOWLEDGEMENTS

We would like to thank EMBO for supporting MAO with a long-term fellowship (ALF-1712005). DT was supported by an LMB Cambridge Student Scholarship. Diffraction data was collected at beamlines ID29, ID23 and ID14 at the ESRF (Grenoble, France) and we would like to thank the beamline staff for excellent support.

TABLES

Table 1: Summary of available FtsZ structures.

Table 2: Residues selected for fitting of the nucleotide-binding domain, rmsd determination and inter-domain angle analysis.

Table 3: Rmsd values between different FtsZ molecules in Å.

Table 4: C-terminal domain rotation angles related to PaFtsZ without SulA.

REFERENCES

1. Bi, E. F. & Lutkenhaus, J. (1991). FtsZ ring structure associated with division in Escherichia coli. *Nature* **354**, 161-4.
2. Stricker, J., Maddox, P., Salmon, E. D. & Erickson, H. P. (2002). Rapid assembly dynamics of the Escherichia coli FtsZ-ring demonstrated by fluorescence recovery after photobleaching. *Proc Natl Acad Sci U S A* **99**, 3171-5.
3. Mukherjee, A., Dai, K. & Lutkenhaus, J. (1993). Escherichia coli cell division protein FtsZ is a guanine nucleotide binding protein. *Proc Natl Acad Sci U S A* **90**, 1053-7.
4. Bramhill, D. & Thompson, C. M. (1994). GTP-dependent polymerization of Escherichia coli FtsZ protein to form tubules. *Proc Natl Acad Sci U S A* **91**, 5813-7.
5. Romberg, L. & Levin, P. A. (2003). Assembly dynamics of the bacterial cell division protein FTSZ: poised at the edge of stability. *Annu Rev Microbiol* **57**, 125-54.
6. Errington, J., Daniel, R. A. & Scheffers, D. J. (2003). Cytokinesis in bacteria. *Microbiol Mol Biol Rev* **67**, 52-65, table of contents.
7. Weiss, D. S. (2004). Bacterial cell division and the septal ring. *Mol Microbiol* **54**, 588-97.
8. Michie, K. A. & Löwe, J. (2006). Dynamic filaments of the bacterial cytoskeleton. *Annu Rev Biochem* **75**, 467-92.
9. Graumann, P. L. (2006). Cytoskeletal Elements in Bacteria. *Annu Rev Microbiol*.
10. Varma, A. & Young, K. D. (2004). FtsZ collaborates with penicillin binding proteins to generate bacterial cell shape in Escherichia coli. *J Bacteriol* **186**, 6768-74.
11. Aaron, M., Charbon, G., Lam, H., Schwarz, H., Vollmer, W. & Jacobs-Wagner, C. (2007). The tubulin homologue FtsZ contributes to cell elongation by guiding cell wall precursor synthesis in Caulobacter crescentus. *Mol Microbiol* **64**, 938-52.
12. Varma, A., de Pedro, M. & Young, K. D. (2007). FtsZ directs a second mode of peptidoglycan synthesis in Escherichia coli. *J Bacteriol*.
13. Löwe, J. & Amos, L. A. (1998). Crystal structure of the bacterial cell-division protein FtsZ. *Nature* **391**, 203-6.
14. Nogales, E., Wolf, S. G. & Downing, K. H. (1998). Structure of the alpha beta tubulin dimer by electron crystallography. *Nature* **391**, 199-203.
15. Nogales, E., Downing, K. H., Amos, L. A. & Löwe, J. (1998). Tubulin and FtsZ form a distinct family of GTPases. *Nat Struct Biol* **5**, 451-8.
16. Desai, A. & Mitchison, T. J. (1997). Microtubule polymerization dynamics. *Annu Rev Cell Dev Biol* **13**, 83-117.
17. Molodtsov, M. I., Grishchuk, E. L., Efremov, A. K., McIntosh, J. R. & Ataullakhanov, F. I. (2005). Force production by depolymerizing microtubules: a theoretical study. *Proc Natl Acad Sci U S A* **102**, 4353-8.

18. Westermann, S., Wang, H. W., Avila-Sakar, A., Drubin, D. G., Nogales, E. & Barnes, G. (2006). The Dam1 kinetochore ring complex moves processively on depolymerizing microtubule ends. *Nature* **440**, 565-9.
19. Gonzalez, J. M., Jimenez, M., Velez, M., Mingorance, J., Andreu, J. M., Vicente, M. & Rivas, G. (2003). Essential cell division protein FtsZ assembles into one monomer-thick ribbons under conditions resembling the crowded intracellular environment. *J Biol Chem* **278**, 37664-71.
20. Oliva, M. A., Huecas, S., Palacios, J. M., Martin-Benito, J., Valpuesta, J. M. & Andreu, J. M. (2003). Assembly of archaeal cell division protein FtsZ and a GTPase-inactive mutant into double-stranded filaments. *J Biol Chem* **278**, 33562-70.
21. Lu, C., Reedy, M. & Erickson, H. P. (2000). Straight and curved conformations of FtsZ are regulated by GTP hydrolysis. *J Bacteriol* **182**, 164-70.
22. Huecas, S. & Andreu, J. M. (2004). Polymerization of nucleotide-free, GDP- and GTP-bound cell division protein FtsZ: GDP makes the difference. *FEBS Lett* **569**, 43-8.
23. Mingorance, J., Rueda, S., Gomez-Puertas, P., Valencia, A. & Vicente, M. (2001). Escherichia coli FtsZ polymers contain mostly GTP and have a high nucleotide turnover. *Mol Microbiol* **41**, 83-91.
24. Chen, Y. & Erickson, H. P. (2005). Rapid in vitro assembly dynamics and subunit turnover of FtsZ demonstrated by fluorescence resonance energy transfer. *J Biol Chem* **280**, 22549-54.
25. Li, H., DeRosier, D. J., Nicholson, W. V., Nogales, E. & Downing, K. H. (2002). Microtubule structure at 8 A resolution. *Structure* **10**, 1317-28.
26. Ravelli, R. B., Gigant, B., Curmi, P. A., Jourdain, I., Lachkar, S., Sobel, A. & Knossow, M. (2004). Insight into tubulin regulation from a complex with colchicine and a stathmin-like domain. *Nature* **428**, 198-202.
27. Wang, H. W. & Nogales, E. (2005). Nucleotide-dependent bending flexibility of tubulin regulates microtubule assembly. *Nature* **435**, 911-5.
28. Aldaz, H., Rice, L. M., Stearns, T. & Agard, D. A. (2005). Insights into microtubule nucleation from the crystal structure of human gamma-tubulin. *Nature* **435**, 523-7.
29. Schlieper, D., Oliva, M. A., Andreu, J. M. & Löwe, J. (2005). Structure of bacterial tubulin BtubA/B: evidence for horizontal gene transfer. *Proc Natl Acad Sci U S A* **102**, 9170-5.
30. Schlichting, I., Almo, S. C., Rapp, G., Wilson, K., Petratos, K., Lentfer, A., Wittinghofer, A., Kabsch, W., Pai, E. F., Petsko, G. A. & et al. (1990). Time-resolved X-ray crystallographic study of the conformational change in Ha-Ras p21 protein on GTP hydrolysis. *Nature* **345**, 309-15.
31. Wittinghofer, A. & Pai, E. F. (1991). The structure of Ras protein: a model for a universal molecular switch. *Trends Biochem Sci* **16**, 382-7.
32. Kjeldgaard, M., Nissen, P., Thirup, S. & Nyborg, J. (1993). The crystal structure of elongation factor EF-Tu from Thermus aquaticus in the GTP conformation. *Structure* **1**, 35-50.
33. Roll-Mecak, A., Cao, C., Dever, T. E. & Burley, S. K. (2000). X-Ray structures of the universal translation initiation factor IF2/eIF5B: conformational changes on GDP and GTP binding. *Cell* **103**, 781-92.

34. Nogales, E. & Wang, H. W. (2006). Structural mechanisms underlying nucleotide-dependent self-assembly of tubulin and its relatives. *Curr Opin Struct Biol* **16**, 221-9.
35. Nogales, E. & Wang, H. W. (2006). Structural intermediates in microtubule assembly and disassembly: how and why? *Curr Opin Cell Biol* **18**, 179-84.
36. Oliva, M. A., Cordell, S. C. & Löwe, J. (2004). Structural insights into FtsZ protofilament formation. *Nat Struct Mol Biol* **11**, 1243-50.
37. Buey, R. M., Diaz, J. F. & Andreu, J. M. (2006). The nucleotide switch of tubulin and microtubule assembly: a polymerization-driven structural change. *Biochemistry* **45**, 5933-8.
38. Urgaonkar, S., La Pierre, H. S., Meir, I., Lund, H., RayChaudhuri, D. & Shaw, J. T. (2005). Synthesis of antimicrobial natural products targeting FtsZ: (+/-)-dichamanetin and (+/-)-2' "-hydroxy-5' '-benzylisouvarinol-B. *Org Lett* **7**, 5609-12.
39. Erickson, H. P., Taylor, D. W., Taylor, K. A. & Bramhill, D. (1996). Bacterial cell division protein FtsZ assembles into protofilament sheets and minirings, structural homologs of tubulin polymers. *Proc Natl Acad Sci U S A* **93**, 519-23.
40. Hyman, A. A., Chretien, D., Arnal, I. & Wade, R. H. (1995). Structural changes accompanying GTP hydrolysis in microtubules: information from a slowly hydrolyzable analogue guanylyl-(alpha,beta)-methylene-diphosphonate. *J Cell Biol* **128**, 117-25.
41. Wang, H. W., Long, S., Finley, K. R. & Nogales, E. (2005). Assembly of GMPCPP-bound tubulin into helical ribbons and tubes and effect of colchicine. *Cell Cycle* **4**, 1157-60.
42. Cordell, S. C., Robinson, E. J. & Löwe, J. (2003). Crystal structure of the SOS cell division inhibitor SulA and in complex with FtsZ. *Proc Natl Acad Sci U S A* **100**, 7889-94.
43. Mukherjee, A., Cao, C. N. & Lutkenhaus, J. (1998). Inhibition of FtsZ polymerization by SulA, an inhibitor of septation in Escherichia coli. *Proceedings of the National Academy of Sciences of the United States of America* **95**, 2885-2890.
44. Nicholson, W. V., Lee, M., Downing, K. H. & Nogales, E. (1999). Cryo-electron microscopy of GDP-tubulin rings. *Cell Biochem Biophys* **31**, 175-83.
45. Rivas, G., Lopez, A., Mingorance, J., Ferrandiz, M. J., Zorrilla, S., Minton, A. P., Vicente, M. & Andreu, J. M. (2000). Magnesium-induced linear self-association of the FtsZ bacterial cell division protein monomer. The primary steps for FtsZ assembly. *J Biol Chem* **275**, 11740-9.
46. Stock, D., Perisic, O. & Löwe, J. (2005). Robotic nanolitre protein crystallisation at the MRC Laboratory of Molecular Biology. *Prog Biophys Mol Biol* **88**, 311-27.
47. Collaborative_Computational_Project_Number_4. (1994). The CCP4 suite: Programs for protein crystallography. *Acta Crystallogr D Biol Crystallogr* **D50**.
48. Brunger, A. T., Adams, P. D., Clore, G. M., DeLano, W. L., Gros, P., Grosse-Kunstleve, R. W., Jiang, J. S., Kuszewski, J., Nilges, M., Pannu, N. S., Read, R. J., Rice, L. M., Simonson, T. & Warren, G. L. (1998). Crystallography & NMR system: A new software suite for macromolecular structure determination. *Acta Crystallogr D Biol Crystallogr* **54**, 905-21.

49. Murshudov, G. N., Vagin, A. A. & Dodson, E. J. (1997). Refinement of macromolecular structures by the maximum-likelihood method. *Acta Crystallogr D Biol Crystallogr* **53**, 240-55.
50. Krissinel, E. & Henrick, K. (2004). Secondary-structure matching (SSM), a new tool for fast protein structure alignment in three dimensions. *Acta Crystallogr D Biol Crystallogr* **60**, 2256-68.

Figure 1

A

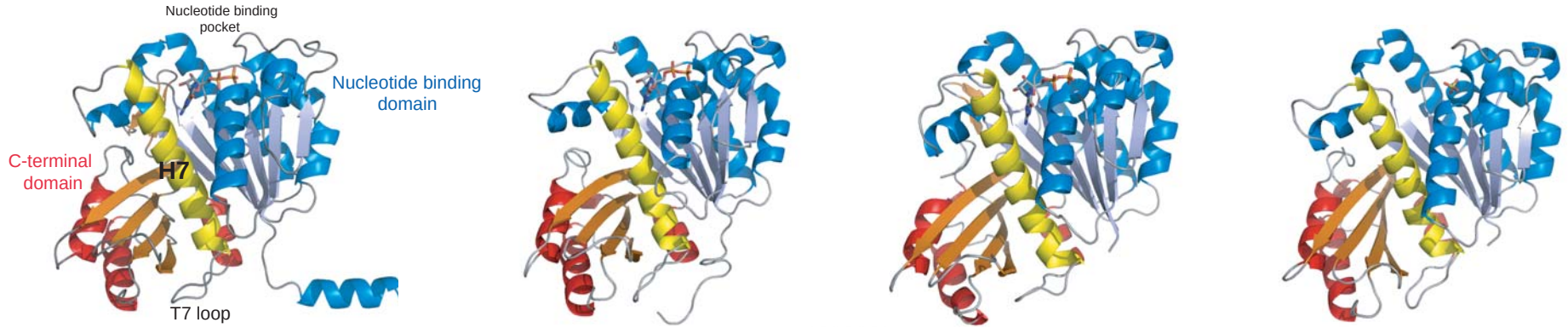
Nucleotide binding pocket
Nucleotide binding domain
C-terminal domain
H7
T7 loop
M. jannaschii
P. aeruginosa
A. aeolicus
B. subtilis

B

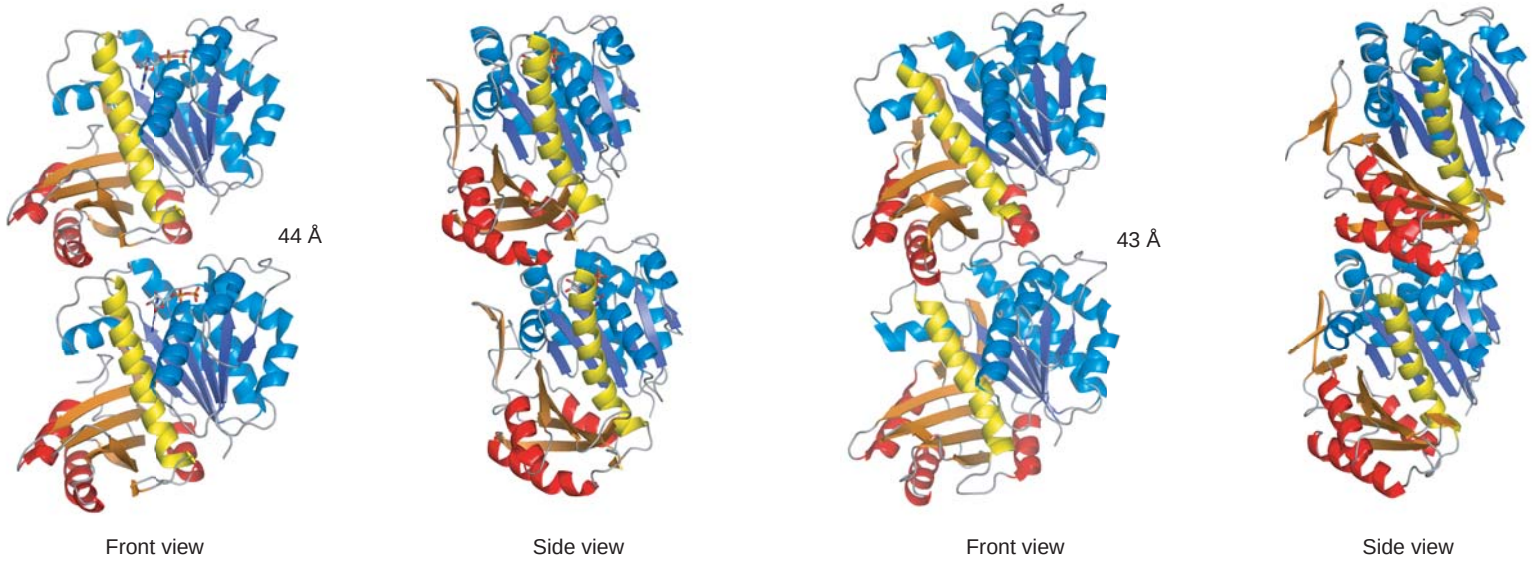
44 Å
43 Å
Front view
Side view
Front view
Side view
A. aeolicus
M. jannaschii

Figure 2

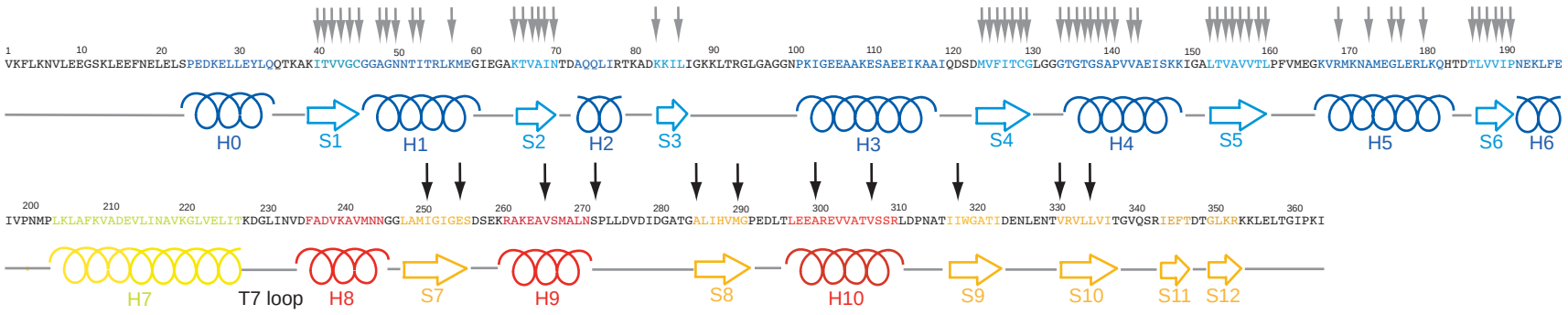
VKFLKNVLEEGSKLEEFNELELSPEDKELLEYLQQTKAKITVVGCGGAGNNTITRLKMEGIEGAKTVAINTDAQQLIRTKADKKILIGKKLTRGLGAGGNPKIGEEAAKESAEEIKAAIQDSDMVFITCGLGGGTGTGSAPVVAEISKKIGALTVAVVTLPFVMEGKVRMKNAMEGLERLKQHTDTLVVIPNEKLFE
H0
S1
H1
S2
H2
S3
H3
S4
H4
S5
H5
S6
H6
IVPNMPLKLAFKVADEVLINAVKGLVELITKDGLINVDFADVKAVMNNGGLAMIGIGESDSEKRAKEAVSMALNSPLLDVDIDGATGALIHVMGPEDLTLEEAREVVATVSSRLDPNATIIWGATIDENLENTVRVLLVITGVQSRIEFTDTGLKRKKLELTGIPKI
H7
T7 loop
H8
S7
H9
S8
H10
S9
S10
S11
S12

Figure 3

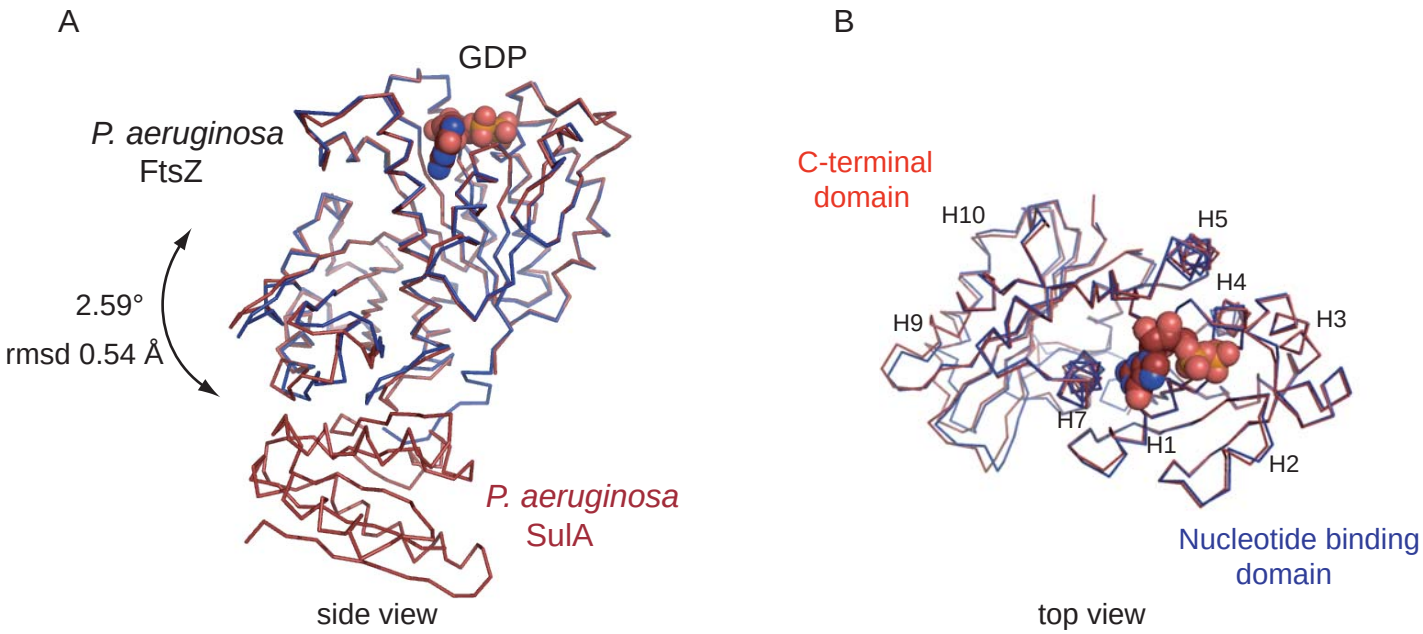
A
GDP
P. aeruginosa
FtsZ
2.59°
rmsd 0.54 Å
P. aeruginosa
SulA
side view
B
C-terminal
domain
H10
H5
H4
H9
H3
H7
H1
H2
Nucleotide binding
domain
top view

Figure 4

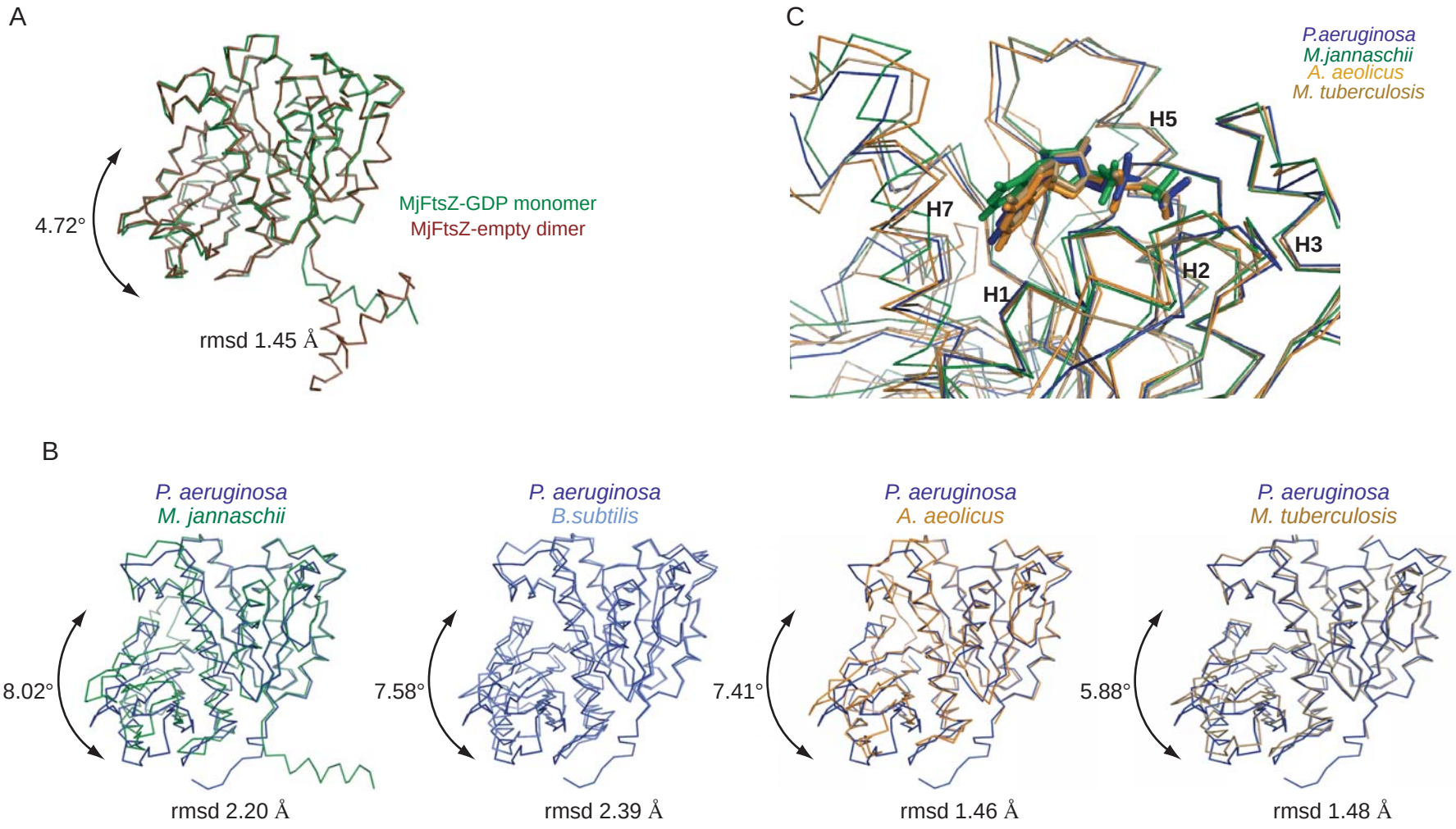
A
4.72°
MjFtsZ-GDP monomer
MjFtsZ-empty dimer
rmsd 1.45 Å
C
P.aeruginosa
M.jannaschii
A. aeolicus
M. tuberculosis
H5
H7
H3
H2
H1
B
P. aeruginosa
M. jannaschii
8.02°
rmsd 2.20 Å
P. aeruginosa
B.subtilis
7.58°
rmsd 2.39 Å
P. aeruginosa
A. aeolicus
7.41°
rmsd 1.46 Å
P. aeruginosa
M. tuberculosis
5.88°
rmsd 1.48 Å

Figure 5

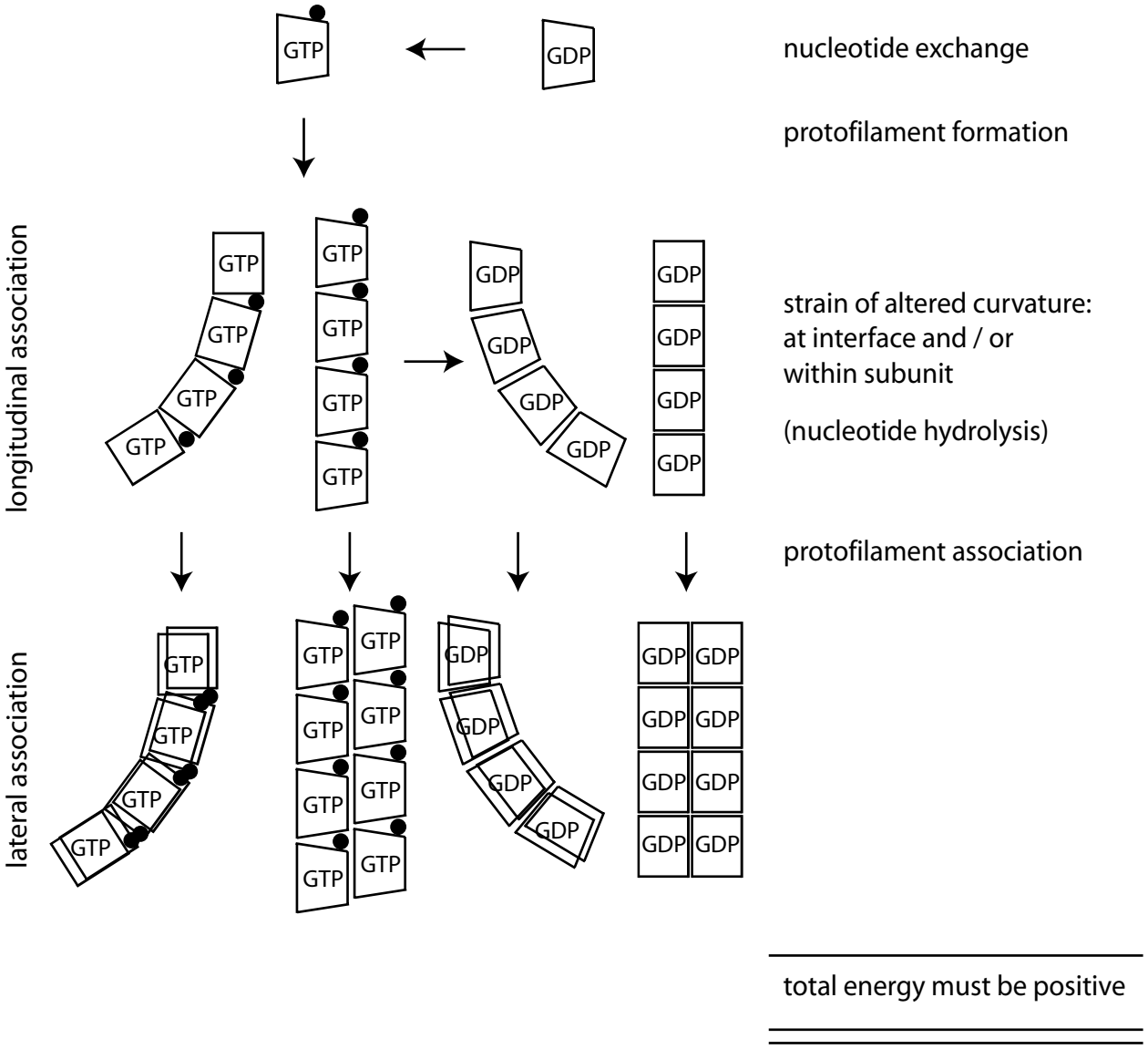
GTP
GDP
nucleotide exchange
protofilament formation
longitudinal association
strain of altered curvature:
at interface and / or
within subunit
(nucleotide hydrolysis)
protofilament association
lateral association
total energy must be positive

Table 1: Summary of FtsZ structures used/solved in this study.

Methanococcus jannaschii							
PDB entry	MJZ	1FSZ	1W58	1W59	1W5B	1W5A	1W5E
Protein length	364 (C-terminal His-tag protein)	364 (C-terminal His-tag protein)	364 (C-terminal His-tag protein)	364 (C-terminal His-tag protein)	364 (C-terminal His-tag protein)	364 (C-terminal His-tag protein)	364 (mutation W319Y, no tag)
Purification method	Ni-NTA affinity chromatography under denaturing conditions, refolded and gel filtration	Ni-NTA affinity cromatography and gel filtration	Ni-NTA affinity cromatography and gel filtration	Ni-NTA affinity chromatography under denaturing conditions, refolded and gel filtration	Ni-NTA affinity chromatography under denaturing conditions, refolded and gel filtration	Ni-NTA affinity chromatography under denaturing conditions, refolded and gel filtration	HiTrap-Q anion exchange chromatography, HiTrap Phenyl Sepharose HP hydrophobic chromatography and gel filtration
Space group	$P3_121$	$I2_13$	$I2_13$	$P2_1$	$P2_1$	$P2_1$	P1
Resolution (Å)	1.7 Å	2.8	2.5	2.7	2.2	2.4	3.0
Chains per asymmetric unit	1 (monomer)	1 (monomer)	1 (monomer)	2 (longitudinal dimer)	2 (longitudinal dimer)	2 (longitudinal dimer)	9 (monomer)
R	0.179	0.199	0.221	0.216	0.209	0.218	0.264
Rfree	0.208	0.282	0.253	0.296	0.259	0.264	0.298
Nucleotide binding site	GDP	GDP	GMPCPP/ Mg^{2+} (soak of 1FSZ)	No nucleotide but SO_4^- in both chains	GTP in both chains (soak of 1W59)	GTP/Mg^{2+} chain A GTP chain B (soak of 1W59)	GTP all the chains
Chain ordered in the unit cell	20-354	23-356	23-363	A 3-17, 20-354 B 22-364	A 22-355 B 22-357	A 22-355 B 22-357	23-354 chains A,C,D,F,G,I 23-355 chains B, E, H

	Pseudomonas aeruginosa		*Mycobacterium tuberculosis*			*Thermotoga maritima*	*Bacillus subtilis*	*Aquifex aeolicus*
PDB entry	1OFU	PAZ	1RQ2	1RQ7	1RLU	1W5F	BSZ	AAZ
Protein length	318 (full length protein 394, N-terminal Strep-tag and C-terminal His-tag)	318 (full length protein 394, N-terminal Strep-tag and C-terminal His-tag)	379 (N-terminal His-tag)	379 (N-terminal His-tag)	379 (N-terminal His-tag)	351 (T7 loop change from 217 to IRLTSRFARIE, C-terminal His-tag)	382 (no tag)	331 (full length 368, C-terminal His-tag
Purification method	Ni-NTA affinity cromatography and gel filtration	HiTrap Q anion exchange chromatography and gel filtration	Ni^{2+} affinity chromatography, trombin His-tag remove and gel filatration	Ni^{2+} affinity chromatography, trombin His-tag remove and gel filatration	Ni^{2+} affinity chromatography, trombin His-tag remove and gel filatration	Ni-NTA affinity cromatography and gel filtration	HiTrap Q anion exchange chromatography and gel filtration	Ni-NTA affinity cromatography and gel filtration
Space group	$P2_12_12_1$	$P6_3$	$P6_5$	$P6_5$	$P6_5$	$P2_12_12$	P321	$P2_1$
Resolution (Å)	2.1	2.9	1.9	2.6	2.0	2.0	2.5	1.8
Chains per asymmetric unit	4 (central dimer of SulA and one FtsZ molecule bind to each SulA	1 (monomer)	2 (lateral dimer)	2 (lateral dimer)	2 (lateral dimer)	2 (domain-swapped dimer)	1 (monomer)	1 (monomer)
R	0.216	0.206	0.187	0.184	0.180	0.203	0.218	0.190
Rfree	0.255	0.316	0.222	0.242	0.224	0.234	0.267	0.225
Nucelotide binding site	GDP	GDP	Citrate chain A Empty chain B	GDP chain A Empty chain B	GTP-γ-S chain A Empty chain B	GMPCPP/ Mg^{2+} both chains	No nucleotide but SO_4^-	GDP
Chain order in the unit cell	A 11-317 B 11.317	2-316	A 8-63, 69-312 B 8-59, 70-169, 174-313	A 8-63, 69-312 B 6-59, 70-170, 174-313	A 8-312 B 6-59, 70-169, 174-312	A 22-337 B 22-337	12-315	4-326

Table 2: Residues selected for aligning the nucleotide-binding domains (top) and for the determination of rmsd values and angles between C-terminal domains (bottom).

Nucleotide-binding domain fitting						
Secondary Structure Element	PaFtsZ	AaFtsZ	BsFtsZ	MtFtsZ	MjFtsZ	TmFtsZ
S1	I14	I6	I14	I11	I40	I24
	K15	K7	K15	K12	T41	K25
	V16	V8	V16	V13	V42	V26
	I17	I9	I17	V14	V43	I27
	G18	G10	G18	G15	G44	G28
	V19	V11	V19	I16	C45	V29
H1	G22	G14	G22	G19	A48	A32
	G23	G15	G23	G20	G49	G33
	G24	S16	N24	V21	N50	N34
	A26	A18	A26	A23	T52	A36
	V27	V19	V27	V24	I53	I37
	A31	Y23	I31	I28	K57	I41
S2	E39	E31	E39	E36	K65	E49
	F40	L32	Y40	F37	T66	F50
	I41	Y33	I41	I38	V67	V51
	C42	A34	A42	A39	A68	A52
	A43	I35	V43	I40	I69	V53
	N44	N36	N44	N41	N70	N54
S3	T57	N49	V57	V54	K83	V67
	Q60	Q52	Q60	D57	L86	Q70
S4	M98	M90	M98	M95	M124	M108
	V99	V91	V99	V96	V125	V109
	F100	F92	F100	F97	F126	F110
	I101	I93	V101	V98	I127	I111
	T102	S94	T102	T99	T128	T112
	T103	A95	A103	A100	C129	A113
	G104	G96	G104	G101	G130	G114
H4	G108	G100	G108	G105	G134	G118
	T109	T101	T109	T106	T135	T119
	G110	G102	G110	G107	G136	G120
	T111	T103	T111	T108	T137	T121
	G112	G104	G112	G109	G138	G122
	A113	A105	A113	G110	S139	A123
	A114	A106	A114	A111	A140	S124
	P115	P107	P115	P112	P141	P125
	I117	I109	I117	V114	V143	I127
	A118	A110	A118	A115	A144	A128
S5	L127	L119	L127	L124	L153	L137
	T128	T120	T128	T125	T154	T138
	V129	V121	V129	V126	V155	V139
	A130	A122	G130	G127	A156	A140
	V131	V123	V131	V128	V157	I141
	V132	A124	V132	V129	V158	V142
	T133	T125	T133	T130	T159	T143
	R134	L126	R134	R131	L160	T144
H5	R143	K135	R143	R140	R169	R153
	A147	A139	A147	A144	A173	A157
	G150	G142	G150	G147	G176	G160
	I151	L143	I151	I148	L177	L161
	L154	L146	M154	L151	L180	L164
S6	S160	A152	T160	T157	T186	T170
	L161	Y153	L161	L158	L187	L171
	I162	I154	I162	I159	V188	I172
	T163	V155	V163	V160	V189	K173
	I164	I156	I164	I161	I190	I174
	P165	H157	P165	P162	P191	S175

rmsd determination and inter-domain angle analysis					
PaFtsZ	AaFtsZ	BsFtsZ	MtFtsZ	MjFtsZ	TmFtsZ
M226	I218	M226	M223	I251	L238
C230	E222	I230	S227	E255	V242
T241	V233	A241	A238	V266	A253
N247	S238	S247	S244	S272	S259
I261	L253	V260	V257	A285	I272
T266	W258	T265	A262	M290	T277
Y276	V268	V275	I272	A300	V287
I283	I275	V282	V279	V307	I294
K294	I286	I293	I290	I318	K305
L307	I299	I306	V303	V331	I319
V313	I303	V310	V307	L335	F323

Table 3

Table 3: Rmsd values of key residues in the C-terminal domain after alignment of the N-terminal domains.

Methanococcus jannaschii																	
2W58	AW59	BW59	AW5B	BW5B	AW5A	BW5A	AW5E	BW5E	CW5E	DW5E	EW5E	FW5E	GW5E	HW5E	IW5E	MJZ	PDB entry
0.393	1.45	1.469	0.995	0.997	0.964	0.971	1.058	1.060	1.040	1.065	1.088	1.047	1.053	1.062	1.050	1.209	1FSZ
--------	1.578	1.604	1.074	1.079	1.034	1.046	1.193	1.188	1.166	1.195	1.211	1.167	1.188	1.190	1.171	1.240	1W58
	--------	0.118	0.591	0.561	0.620	0.598	0.551	0.555	0.601	0.540	0.523	0.577	0.554	0.552	0.585	0.609	AW59
		-------	0.637	0.596	0.655	0.631	0.587	0.593	0.636	0.573	0.555	0.609	0.589	0.585	0.619	0.646	BW59
			-------	0.207	0.139	0.194	0.409	0.402	0.422	0.399	0.398	0.393	0.401	0.403	0.406	0.405	AW5B
				-------	0.227	0.169	0.388	0.397	0.432	0.387	0.403	0.421	0.382	0.396	0.421	0.360	BW5B
					--------	0.088	0.417	0.421	0.432	0.401	0.404	0.403	0.411	0.411	0.415	0.379	AW5A
						--------	0.394	0.393	0.421	0.378	0.385	0.395	0.389	0.392	0.404	0.358	BW5A
							--------	0.089	0.165	0.073	0.126	0.163	0.053	0.098	0.159	0.523	AW5E
								--------	0.112	0.109	0.097	0.113	0.096	0.052	0.108	0.513	BW5E
									--------	0.183	0.166	0.09	0.165	0.119	0.058	0.558	CW5E
										-------	0.090	0.154	0.084	0.105	0.166	0.504	DW5E
											--------	0.115	0.134	0.090	0.144	0.492	EW5E
												--------	0.160	0.104	0.065	0.527	FW5E
													--------	0.086	0.150	0.513	GW5E
														--------	0.095	0.505	HW5E
															---------	0.532	IW5E

Pseudomonas aeruginosa			*Mycobacterium tuberculosis*			*Aquifex aeolicus*	*Bacillus subtilis*		
1OFU-A	1OFU-B	1PAZ-A	1RQ2-A	1RQ7-A	1RLU-A	AAZ-A	BSZ-A	PDB entry	
2.151	2.784	2.202	1.607	1.782	1.759	1.453	2.149	1FSZ	
2.065	2.687	2.117	1.612	1.778	1.761	1.365	2.212	1W58	
2.751	3.316	2.875	1.787	1.958	1.886	1.946	1.409	1W59-A	
2.774	3.342	2.896	1.815	1.983	1.911	1.988	1.425	BW59-B	
2.467	3.064	2.582	1.574	1.775	1.715	1.659	1.568	AW5B-A	
2.316	2.910	2.428	1.437	1.620	1.557	1.538	1.410	BW5B-B	
2.408	3.012	2.521	1.537	1.733	1.673	1.620	1.551	AW5A-A	
2.374	2.977	2.489	1.508	1.699	1.638	1.594	1.506	BW5A-B	
2.428	3.009	2.537	1.614	1.797	1.737	1.627	1.514	AW5E-A	*Methanococcus jannaschii*
2.436	3.019	2.584	1.606	1.792	1.731	1.630	1.511	BW5E-B	
2.420	2.998	2.566	1.613	1.800	1.741	1.614	1.542	CW5E-C	
2.449	3.032	2.595	1.637	1.820	1.759	1.644	1.528	DW5E-D	
2.483	3.069	2.634	1.650	1.835	1.774	1.674	1.533	EW5E-E	
2.455	3.042	2.604	1.634	1.822	1.763	1.647	1.559	FW5E-F	
2.417	3.000	2.561	1.593	1.777	1.717	1.615	1.498	GW5E-G	
2.434	3.019	2.582	1.601	1.786	1.726	1.627	1.505	HW5E-H	
2.431	3.012	2.578	1.612	1.799	1.740	1.619	1.535	IW5E-I	
2.389	2.983	2.528	1.462	1.650	1.586	1.618	1.328	MJZ17-A	
--------	0.818	0.541	1.492	1.413	1.433	1.341	2.272	AOFU-A	*Pseudomonas aeruginosa*
	-------	0.894	2.106	1.986	2.018	1.760	2.735	BOFU-B	
		---------	1.580	1.477	1.509	1.455	2.393	1PAZ-A	
			--------	0.259	0.229	1.335	1.218	ARQ2-A	*Mycobacterium tuberculosis*
				-------	0.130	1.376	1.262	ARQ7-A	
					-------	1.382	1.189	ARLU-A	
						-------	1.901	AAZ-A	*Aquifex aeolicus*

Table 4: Angles between C-terminal domains after alignment of the N-terminal domains of FtsZ. After aligning against the averaged reference, angles were calculated relative to PaFtsZ (PDB ID XXXX).

Organism	PDB entry	Rotation angle
Methanococcus jannaschii	1FSZ	8.02º
	1W58	8.26º
	1W59-A	8.24º
	1W59-B	7.88º
	1W5B-A	8.81º
	1W5B-B	7.52º
	1W5A-A	8.33º
	1W5A-B	7.99º
	1W5E-A	8.77º
	1W5E-B	8.81º
	1W5E-C	8.99º
	1W5E-D	8.82º
	1W5E-E	8.89º
	1W5E-F	9.02º
	1W5E-G	8.71º
	1W5E-H	8.77º
	1W5E-I	8.99º
	MJZ17	8.04º
Pseudomonas aeruginosa	1OFU-A	2.59º
	1OFU-B	2.09º
Mycobacterium tuberculosis	1RQ2-A	5.77º
	1RQ7-A	5.88º
	1RLU-A	5.74º
Aquifex aeolicus	AAZ	7.41º
Bacillus subtilis	BSZ	7.58º